

THE LEPTON FLAVOUR VIOLATION DECAYS AT THE LHCb EXPERIMENT*

ANNA OSSOWSKA

on behalf of the LHCb Collaboration

The Henryk Niewodniczański Institute of Nuclear Physics PAN
Radzikowskiego 152, Kraków, Poland

(Received March 26, 2019)

These proceedings present a set of searches for lepton flavour violation, performed using decays of B and D mesons, using data collected by the LHCb experiment. None of the described searches resulted in an observation of the signal and upper limits on the branching fractions are established.

DOI:10.5506/APhysPolB.50.1177

1. Introduction

The Standard Model (SM) of particle physics is one of the most successful theories in physics which describes the fundamental interactions between elementary particles. It is compatible with almost all experimental results. Many rare decays are suppressed or forbidden in the SM *e.g.* lepton flavour violation decays (LFV). It cannot be ignored that the neutrino oscillations indicate the existence of the LFV decays in neutral sector. The LFV decays are allowed in some physics scenarios beyond the SM, such as supernumerary or theory with multiple Higgs doublet [1].

Lepton number/flavour violating decays of B and D mesons are forbidden in the Standard Model (SM), these kind of decays have not yet been observed. Finding the evidence for such decays would be a clear sign of new physics.

2. The LHCb detector

The LHCb detector [2, 3] shown in Fig. 1 is a single-arm forward spectrometer covering the pseudorapidity range of $2 < \eta < 5$, designed to study

* Presented at the Cracow Epiphany Conference on Advances in Heavy Ion Physics, Kraków, Poland, January 8–11 2019.

decays of particles containing b and c quarks. The detector includes a high-precision tracking system consisting of a silicon-strip vertex detector (VELO) surrounding the pp interaction region. The tracking system allows to reconstruct the trajectories of charged particles and to measure their momenta. The spectrometer magnet, required for the momentum measurement of charged particles, is a dipole magnet providing an integrated field of about 4 Tm, which bends charged particles in the horizontal plane. Charged hadrons are identified using two ring-imaging Cherenkov detectors, designed to identify particles associated to low-momentum and high-momentum tracks. The electromagnetic and hadronic calorimeters provide measurements of the energy of electrons, photons and hadrons. Muons are identified by a system of alternating layers of iron and multiwire proportional chambers. The on-line event selection is performed by a trigger system that includes a hardware stage, based on information from the calorimeter and muon systems, followed by a software stage.

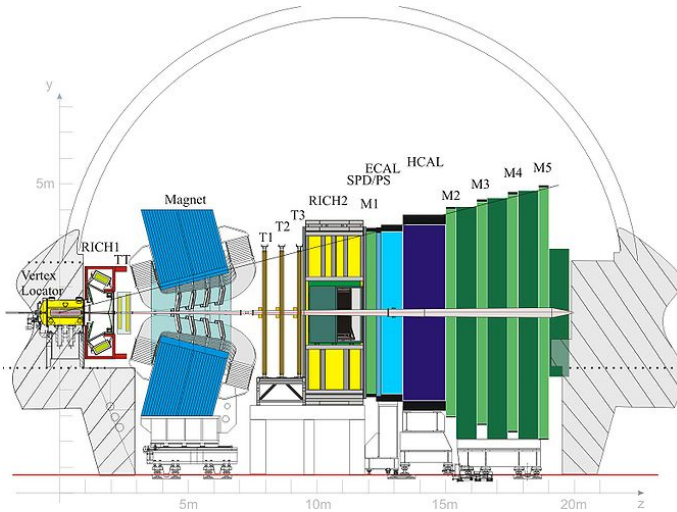


Fig. 1. The model of the LHCb detector [3].

3. Lepton Flavour Violation B and D meson decays

3.1. The search for $B_s^0 \rightarrow e^\pm \mu^\mp$ and $B^0 \rightarrow e^\pm \mu^\mp$ decay

The searches for the LFV in $B_s^0 \rightarrow e^\pm \mu^\mp$ and $B^0 \rightarrow e^\pm \mu^\mp$ decays are performed based on a samples of proton–proton collisions data corresponding to an integrated luminosity of 3 fb^{-1} at the center-of-mass energies of 7 and 8 TeV (Run 1).

The $B^0 \rightarrow K^+\pi^-$ and $B^+ \rightarrow J/\psi(\mu^+\mu^-)K^+$ decays are used as the normalisation channels. The first of them is chosen in view of the similar topology of signal, the second has an abundant yield and a similar purity and trigger selection. The requirements for the normalisation channels are as similar as possible to those used for the signal. Figure 2 presents the invariant mass distribution of these two normalisation channels with fit functions [4].

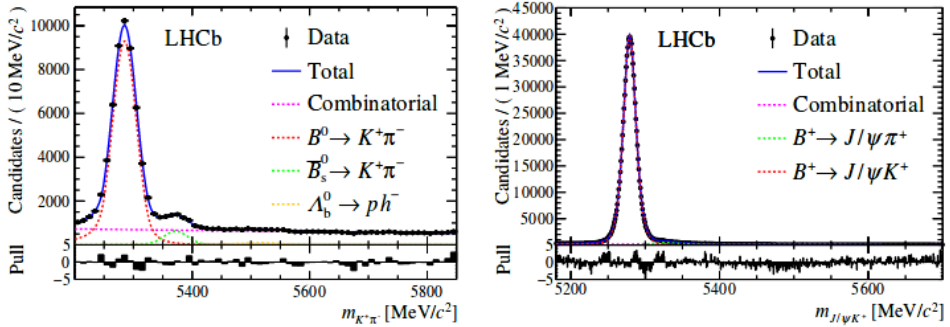


Fig. 2. Invariant mass distributions of the two normalisation channels with fit functions superimposed: (left) and $B^0 \rightarrow K^+\pi^-$ (right) $B^+ \rightarrow J/\psi(\mu^+\mu^-)K^+$ [4].

The data sample is split into two bremsstrahlung categories, first for candidates in which no photon is associated with the electron and the second for candidates in which one or more photons are recovered [4].

The signal region of examined decays is polluted by combinatorial background and by backgrounds from exclusive decays where one or more of the final-state particles are misidentified or not reconstructed. The Boosted Decision Tree (BDT) classifier is used to separate the signal from the combinatorial background. The BDT is trained using the simulated signal of $B^0_{(s)} \rightarrow e^\pm\mu^\mp$, the combinatorial background comes from data sample of the same-sign $e^\pm\mu^\pm$ candidates. The BDT response is shown in Fig. 3.

The shapes of invariant mass distributions of $B^0_{(s)} \rightarrow e^\pm\mu^\mp$ candidates depend on the number of recovered photon. Due to the fact that bremsstrahlung can significantly alter the mass shape by enhancing the tail, the fit model is prepared separately for both bremsstrahlung categories [4]. The modified Crystal Ball Function with two tails on opposite sides is used to modelled the invariant mass distribution. Figure 4 shows the fits of two categories of bremsstrahlung.

No signals of $B^0_{(s)} \rightarrow e^\pm\mu^\mp$ or $B^0 \rightarrow e^\pm\mu^\mp$ decays are observed and the upper limit on branching fraction are steer using the CL_s method. The results of CL_s scan is present in Fig. 5. The background-only expectation is shown by the dashed line, the observed limit is shown as a solid, black line.

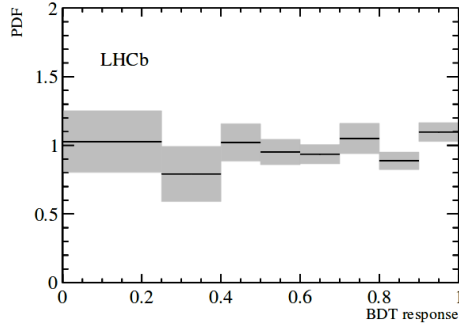


Fig. 3. Expected distribution of the BDT response for $B_{(s)}^0 \rightarrow e^\pm \mu^\mp$ decays with recovered bremsstrahlung photons obtained from the $B^0 \rightarrow K^+ \pi^-$ control channel [4].

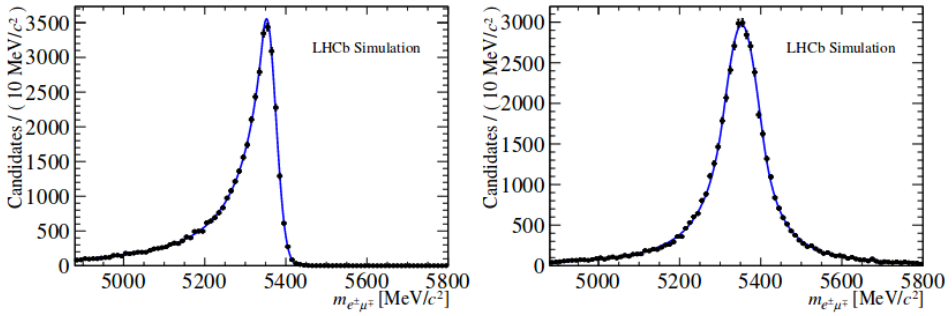


Fig. 4. Left: Invariant mass distribution of simulated $B_{(s)}^0$ candidates with no recovered bremsstrahlung photons. Right: Invariant mass distribution of simulated $B_{(s)}^0$ candidates with one or more recovered bremsstrahlung photons [4].

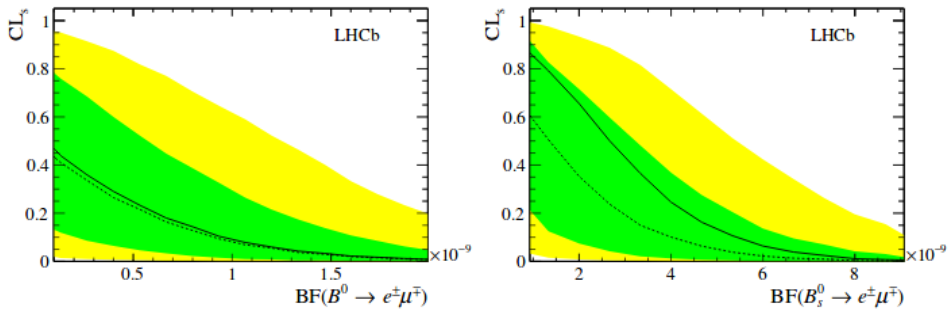


Fig. 5. Left: The upper limit on the branching fraction of $B^0 \rightarrow e^\pm \mu^\mp$. Right: $B_s^0 \rightarrow e^\pm \mu^\mp$ [4].

The upper limits on the branching fraction for $B_s^0 \rightarrow e^\pm \mu^\mp$ are [4]

$$\mathcal{B}(B_s^0 \rightarrow e^\pm \mu^\mp) < 6.3 \times 10^{-9} \text{ at } 95\% \text{ C.L.},$$

$$\mathcal{B}(B^0 \rightarrow e^\pm \mu^\mp) < 1.3 \times 10^{-9} \text{ at } 95\% \text{ C.L.}$$

3.2. The search for $D^0 \rightarrow e^\pm \mu^\mp$ decay

The search is performed with a dataset corresponding to an integrated luminosity of 3 fb^{-1} at proton–proton collisions at the center-of-mass energies of 7 and 8 TeV collected by the LHCb experiment in 2011 and 2012.

The selection of signal candidates is performed by using two decays: first $D^{*+} \rightarrow D^0 \pi^+$ and the second, well-measured normalisation channel $D^0 \rightarrow K^- \pi^+$ with the same topology as the signal. The another decay — $D^0 \rightarrow \pi^+ \pi^-$, where one pion is misidentified as an electron and the other as a muon, is an important source of background. The contamination comes also from the semileptonic mode $D^0 \rightarrow \pi^- e^+ \nu_e$ and $D^0 \rightarrow \pi^- \mu^+ \nu_\mu$. The separation signal from background is performed by using a multivariate classifier — Boosted Decision Tree (BDT), it is trained separately for the 7 and 8 TeV samples [5].

In order to determine the number of signal, the analysis requires the extended maximum likelihood fits, which are made to distribution of $m(D^0)$ and $\Delta m = m(D^{*+}) - m(D^0)$. It is shown in Fig. 6.

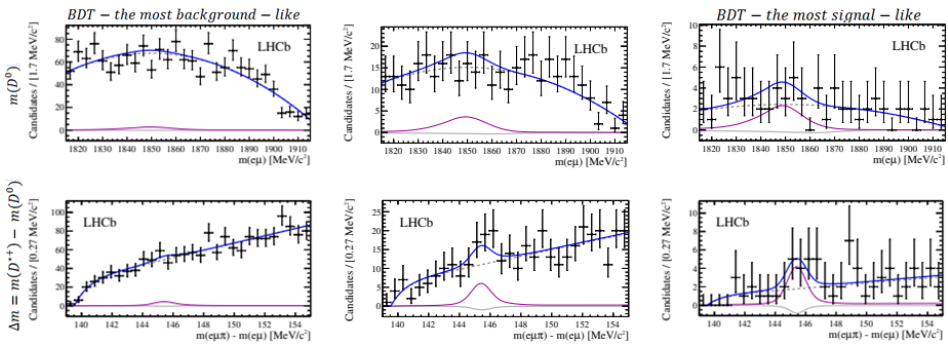


Fig. 6. Distribution of $m(D^0)$ — fist row, distribution of Δm — second row [5].

The first row shows the distribution of $m(D^0)$, the second — $\Delta m = m(D^{*+}) - m(D^0)$ for the $D^0 \rightarrow e^\pm \mu^\mp$ candidates reconstructed in the combined 7 and 8 TeV with fit functions. The columns correspond to 3 bins of BDT output. The solid line shows the total fit.

No evidence is observed for $D^0 \rightarrow e^\pm \mu^\mp$ signal and in that case, the upper limit on the branching fraction is obtained by the CL_s method. Figure 7 shows the distribution of the CL_s method as a function of $\mathcal{B}(D^0 \rightarrow e^\pm \mu^\mp)$.

The expected distribution is shown by the dashed line, the observed by the solid line. The upper limit on the branching fraction for $D^0 \rightarrow e^\pm \mu^\mp$ is

$$\mathcal{B}(D^0 \rightarrow e^\pm \mu^\mp) < 1.6 \times 10^{-8} \text{ at } 95\% \text{ C.L. [5].}$$

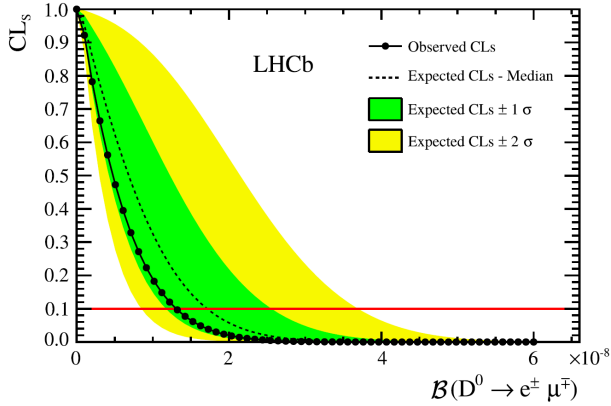


Fig. 7. Distribution of the CL_s method as a function of $\mathcal{B}(D^0 \rightarrow e^\pm \mu^\mp)$ [5].

3.3. The search for $B^- \rightarrow \pi^+ \mu^- \mu^-$ decay

The $B^- \rightarrow \pi^+ \mu^- \mu^-$ decay (Fig. 8) allows to probe Majorana neutrino masses of up to $5 \text{ GeV}/c^2$. The data used for this analysis correspond to an integrated luminosity of 3 fb^{-1} and was collected at a center-of-mass energy of 7 (8) TeV in 2011 (2012), respectively [6].

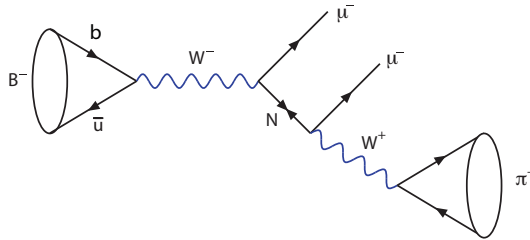


Fig. 8. The Feynman diagram of $B^- \rightarrow \pi^+ \mu^- \mu^-$ decay [6].

The $B^- \rightarrow J/\psi K^-$ decay is used as normalisation channel. The hypothetical neutrino lifetime is scanned in the range of 0–1000 ps split into two ranges. For lifetime $\tau > 1 \text{ ps}$, the $\pi^+ \mu^-$ decay products can appear as significantly detached from the B^- decay vertex. Therefore, the analysis was performed in two strategies: one for short lifetime and another for lifetime up to 1000 ps [6]. This analysis used tracks that begin in the VELO for both of the strategies.

Figure 9 shows the mass spectra of the selected candidates. Backgrounds in the $\pi^+\mu^-\mu^-$ final state come from B decay to charmonium and combinatoric sources. No significant excess of signal events is observed at any of the mass hypothesis, and upper limits on the branching fraction are set by the CL_s method. For neutrino lifetimes shorter than 1 ps an upper limit on $\mathcal{B}(B^- \rightarrow \pi^+\mu^-\mu^-)$ is set as

$$\mathcal{B}(B^- \rightarrow \pi^+\mu^-\mu^-) < 4.0 \times 10^{-9} \text{ at } 95\% \text{ C.L. [6].}$$

This limit is the most restrictive to date [7].

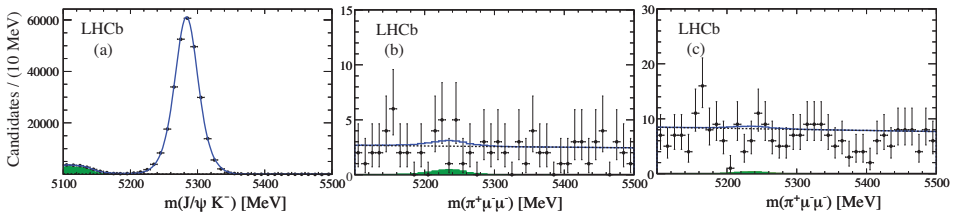


Fig. 9. (Colour on-line) Invariant mass distributions with fits overlaid of candidate mass spectra for $J/\psi K^-$ (left), $\pi^+\mu^-\mu^-$ — for short lifetime (middle), and $\pi^+\mu^-\mu^-$ — for long lifetime (right). Backgrounds that peak under the signal in the middle and right-hand side figure are shaded/green. The dotted lines show the combinatorial backgrounds only, the solid lines show the sum of both backgrounds [6].

The two-dimensional plots of the upper limits on $\mathcal{B}(B^- \rightarrow \pi^+\mu^-\mu^-)$ for several values of neutrino lifetimes are shown in Fig. 10.

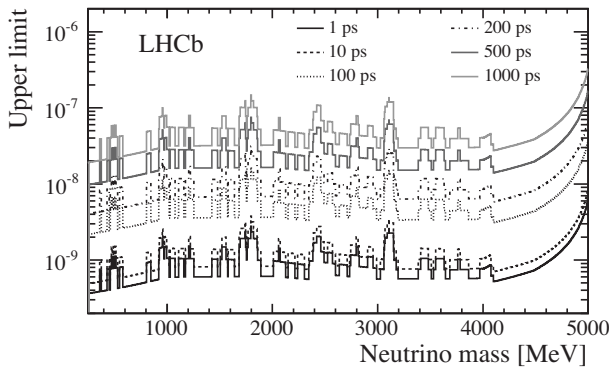


Fig. 10. Upper limits on $B^- \rightarrow \pi^+\mu^-\mu^-$ decays as a function of neutrino mass and neutrino lifetime [6, 7].

4. Summary

In summary, the searches for the lepton flavour violation in B and D meson decays have been presented. No significant excesses are observed for these decays and the upper limits on the branching fractions are set. The searches will be updated and further decay channels will be analyzed with the Run 2 data set.

REFERENCES

- [1] D.H. Perkins, *Introduction to High Energy Physics*, Wydawnictwo Naukowe PWN Warszawa, 2015, ISBN 83-01-14246-4.
- [2] LHCb Collaboration <http://lhcb.web.cern.ch/lhcb/>
- [3] LHCb Collaboration, *JINST* **3**, S08005 (2008).
- [4] LHCb Collaboration, *J. High Energy Phys.* **1803**, 078 (2018) [[arXiv:1710.04111](https://arxiv.org/abs/1710.04111)] [[hep-ex](#)].
- [5] LHCb Collaboration, *Phys. Lett. B* **754**, 167 (2016) [[arXiv:1512.00322](https://arxiv.org/abs/1512.00322)] [[hep-ex](#)].
- [6] R. Aaij *et al.* [LHCb Collaboration], *Phys. Rev. Lett.* **112**, 131802 (2014).
- [7] R. Aaij *et al.* [LHCb Collaboration], *Phys. Rev. D* **85**, 112004 (2012).